Sound & Vibration 2026, 60(3), 3908.
doi: https://doi.org/10.59400/sv3908

Article

Inverse engineering of micro-perforated plates for targeted acoustic characteristics

Binxia Yuan[1,*], Xiangyang Li[1], Tianqi You[1,2], Tianzhong Chen[3], Rui Zhu[1,*]

[1] College of Energy and Mechanical Engineering, Shanghai University of Electric Power, Shanghai 200090, China
[2] Wangting Power Generation Branch, Shanghai Huadian Electric Power Development Co., Ltd., Suzhou 215100, China
[3] Traffic Management Department, Jiangxi Youth Vocational College, Nanchang 330045, China
*** Corresponding author:** Binxia Yuan, yuanbinxia100@163.com; Rui Zhu, zhuruish@163.com

CITATION

Yuan B, Li X, You T, et al. Inverse engineering of micro-perforated plates for targeted acoustic characteristics. Sound & Vibration. 2026; 60(3): 3908. https://doi.org/10.59400/sv3908

ARTICLE INFO

Received: 12 January 2026
Revised: 20 March 2026
Accepted: 23 March 2026
Available online: 27 April 2026

Abstract: The inverse design of micro-perforated panels (MPPs) for target sound absorption remains challenging due to the complex nonlinear relationship between structural parameters and acoustic performance. This study proposes a tandem neural network (TNN) framework to achieve efficient inverse design of single-layer MPPs. A forward multi-layer perceptron (MLP) is first trained to accurately predict the absorption coefficient curve from three key structural parameters: perforation diameter, panel thickness, and cavity depth. The forward model achieves superior accuracy compared to GA-SVR, GridSearch-SVR, and random forest models, with an R^2 of 0.999 and MAE of 0.007. Subsequently, an inverse design network is connected in series with the frozen forward network, taking a target absorption curve as input and outputting the corresponding structural parameters. The activation function of the output layer constrains the parameters within physically feasible ranges. The framework is validated by designing an MPP with a distinct absorption peak in the 300–600 Hz range. The predicted parameters (diameter 0.93 mm, thickness 0.9 mm, cavity depth 9.9 mm) yield an absorption curve that matches the target with an R^2 of 0.997. This work demonstrates that deep learning can effectively automate the inverse design of MPPs, offering a flexible and efficient alternative to traditional trial-and-error methods.

Keywords: micro-perforated panels; multi-layer perceptron; deep learning; inverse design; acoustic performance

1. Introduction

Due to China's rapid urbanization, power substations originally located in rural areas or suburban districts have gradually been relocated to urban areas, making the noise problem more prominent. The research indicates that the transformer's noise is primarily caused by vibrations with frequencies below 500 Hz, particularly at 300 Hz, 100 Hz, and 50 Hz [1]. Micro-perforated panels (MPPs) have a wide sound absorption frequency band and exhibit excellent low-frequency sound absorption performance [2,3]. By adjusting structural parameters, MPPs can achieve efficient sound absorption within specific frequency ranges, with sound absorption coefficients exceeding 95%. The sound absorption performance of MPPs is influenced by four structural parameters: micro-hole aperture, panel thickness, back cavity depth, and perforation rate. Typically, the micro-hole aperture and panel thickness are below 1 mm, and the back cavity depth should not be excessively large. Although numerous novel methods [4, 5] have been

developed for designing structural parameters of MPPs, which significantly outperform traditional approaches, it remains challenging to determine design parameter values based on target sound absorption coefficient curves.

Since Maa's pioneering work [6], a model for predicting single-layer MPPs' sound absorption has been established. However, although these models provided accurate forward predictions, determining the inverse design of structural parameters from the required sound absorption curve is not simple. In contrast, data-driven methods such as neural networks can learn implicit mappings between structural parameters and acoustic performance, enabling fast and flexible inverse design. In recent years, data-driven approaches have emerged as powerful tools for both forward prediction and inverse design in acoustics and metamaterials. Multi-Layer Perceptron's (MLPs) have been applied to predict band gaps, dispersion curves, sound absorption coefficients, energy band features, and material characteristics [7–10]. By using characteristic parameters as inputs and material properties as outputs, MLPs can be trained to achieve high-precision predictions. Meantime, MLPs can also be used for inverse design of acoustic metamaterials, where target properties are taken as inputs and design variables as outputs for training [11, 12]. Zhang et al. [13] used TNN for three-dimensional hybrid-size cavity-based acoustic metamaterials for broadband underwater sound absorption. He et al. [14] achieved inverse design of beam geometry with target topological features by applying deep serial neural networks. Zhang et al. [15] proposed a more accurate Integrated Deep Neural Network (IDNN) model, which integrated multiple deep neural network models to achieve efficient forward and inverse predictions for micro-perforated plate design. Gao et al. [16] demonstrated CNN-based inverse design of a composite acoustic sink, validated experimentally on 79,730 samples, confirming deep learning's applicability to complex acoustic structures. Mahesh et al. [17] proposed a deep neural network-based inverse prediction mechanism for geometrically designing a Helmholtz resonator. Based on backpropagation algorithms, Tandem Neural Network (TNN) searches for appropriate geometric parameters by adjusting the internal parameters of the inverse design network, ensuring that predicted results match target values [18–20]. Generative adversarial networks have also been applied to acoustic metamaterial inverse design; Yan et al. [21] demonstrated a conditional GAN for metaporous materials with perforated plates, achieving experimentally validated broadband absorption. Jiang et al. [22] proposed a VAE-PINN hybrid model for multi-parallel MPP inverse design, incorporating acoustic physics constraints into the loss function to achieve stable parameter derivation with 500,000 training samples and experimental validation.

Among these deep learning approaches, TNN has shown particular promise for inverse design problems due to its ability to decouple the forward and inverse mappings [18–20]. Unlike end-to-end models that directly predict parameters from targets, TNNs leverage a pre-trained forward network as a physics-aware regularizer, ensuring that the predicted parameters produce physically consistent responses. This architecture is especially advantageous when the forward problem is well-understood (as with MPPs), but the inverse problem is ill-posed. The present study adopts this TNN framework, adapting it specifically for single-layer MPP inverse design.

The main objective of this article is to break the traditional forward design pattern of designing the structure first and then testing performance, and achieve performance customization through inverse design. Based on the actual sound absorption application scenarios of power plants, directly design porous structural parameters that can meet the target performance through inverse design. The traditional design method relies on experience or experimental trial and error, with long cycles and high costs. This article combines inverse design with Comsol numerical simulation to quickly deduce structural schemes from performance targets, reducing the number of physical experiments and facilitating the rapid design of perforated plates.

2. Method

2.1. Multilayer perceptron

MLP is a type of feedforward artificial neural network characterized by its fully connected neurons, nonlinear activation functions, and an architecture consisting of at least three layers [23, 24]. MLP can be regarded as a composite function composed of multiple simple functions. By adjusting weights and biases, it can approximate any function and demonstrate powerful nonlinear modeling capabilities.

The MLP architecture has three neurons, corresponding to the panel thickness (t), perforation diameter (d), and cavity depth (H). Three hidden layers are 1,024, 512, and 256 neurons, respectively. The output layer is 156 neurons, corresponding to the discretized absorption coefficients. The number of hidden layers and neurons was determined through systematic hyperparameter tuning, balancing model capacity and generalization performance. Each hidden layer is followed by batch normalization and ReLU activation, which accelerate convergence and introduce nonlinearity. The output layer uses a linear activation function to allow the full range of absorption coefficient values (0 to 1). The total number of trainable parameters in the forward MLP is about 1.2 million.

2.2. Tandem neural network

TNN is specifically designed to address inverse problems. It typically consists of an inverse design network and a pre-trained forward network. The pre-trained forward network is usually an MLP. TNN effectively solves the issue of design variable constraints by introducing a constraint mechanism into the activation function of the inverse design network output layer, ensuring that design variables remain within the traditional optimization domain.

This model adopts a staged training strategy. First, a supervised learning-based feedforward network is constructed to establish a deterministic mapping between structural parameters and properties. The feedforward network parameters are frozen, and adaptive optimization algorithms such as Adam and RMSProp are employed to adjust the inverse design network parameters. The optimization is performed using a loss function based on the mean squared error between the predicted and target responses. Second, the sound absorption coefficient is used as input at the network architecture level, and the constrained design variables are extracted through the

intermediate layer of the inverse design network, coupled with a pretrained feedforward network for attribute verification. In this process, the output response of the pre-trained network serves as an implicit supervision signal, forming a unique unsupervised training paradigm. During the inverse design, the design variables are iteratively refined using the backpropagation algorithm until the predicted properties from the feedforward network converge to the target values. Simultaneously, strictly maintain the frozen parameters of the pretrained feed-forward network to ensure physical consistency during the forward prediction process. It not only guarantees model interpretability but also significantly enhances the efficiency of inverse design for complex systems.

The output of the inverse design network to the input of an MLP (forward analog network) for forward prediction is connected. Meanwhile, the inverse design network output layer activation function is used to limit the range of design parameter values. The combination forms the TNN, as shown in **Figure 1**.

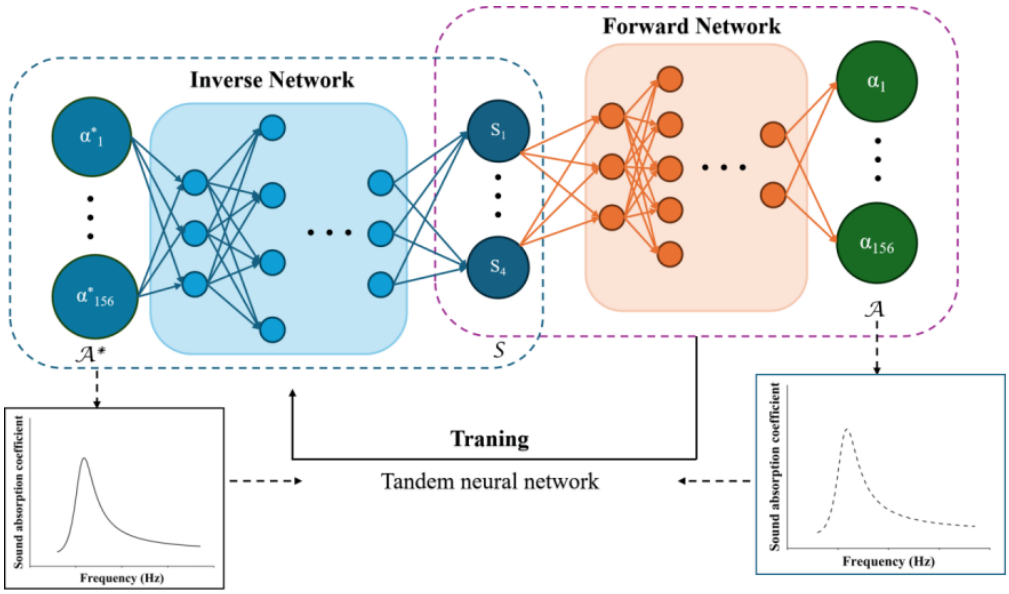

Figure 1. TNN Schematic Diagram.

The inverse network architecture is designed through preliminary experiments. It consists of four hidden layers with 512, 512, 256, and 3 neurons, respectively. Except for the output layer, each layer undergoes batch normalization and ReLU activation. The output layer uses S-shaped activation to constrain three structural parameters within their physical range (d and t are 0.1–1 mm, d is 1–10 mm). The network is trained using the Adam optimizer for 1,000 iteration cycles with a learning rate of 0.001. To prevent overfitting, an early stopping criterion is applied for 50 iteration cycles.

2.3. Evaluation methods for models

R^2 measures the proportion of variance in the true values explained by the predictions, with values closer to 1 indicating a better fit. RMSE quantifies the average magnitude of prediction errors in the same units as the target variable, while MAE provides a more robust measure less sensitive to outliers. Together, these three metrics offer a comprehensive assessment of model accuracy.

To evaluate the accuracy of the model, coefficients of determination (R^2), mean Absolute Error (MAE), and root mean squared error (RMSE) are calculated. The model accuracy is evaluated using R^2, MAE, and RMSE, as defined in Equations (1)–(3).

$$R^2 = \frac{[\sum_{i=1}^{n}(y_i - \bar{y})(y_i^* - \bar{y_i^*})]^2}{\sum_{i=1}^{n}(y_i - \bar{y})^2 \sum_{i=1}^{n}(y_i^* - \bar{y_i^*})^2} \tag{1}$$

$$\text{MAB} = \frac{1}{n}\sum_{i=1}^{n}|y_i - \bar{y}| \tag{2}$$

$$\text{RMSK} = \sqrt{\frac{1}{n}\sum_{i=1}^{n}(y_i - y_i^*)^2} \tag{3}$$

In this formula, n represents the sample size, y_i denotes the observed values of the dependent variable, y_i^* signifies the predicted values of the dependent variable, $\bar{y}$ is the mean of the observed values of the dependent variable, and $\bar{y_i^*}$ is the mean of the predicted values of the dependent variable. The smaller the values of MAE and RMSE, and the closer the R^2 value is to 1, the more accurate the prediction results.

3. Model construction method

In the study of the acoustic characteristics of MPPs, the forward prediction network and the inverse design network complement each other, jointly advancing the understanding of the relationship between MPPs' structure and sound absorption performance. The overall design process is shown in **Figure 2**.

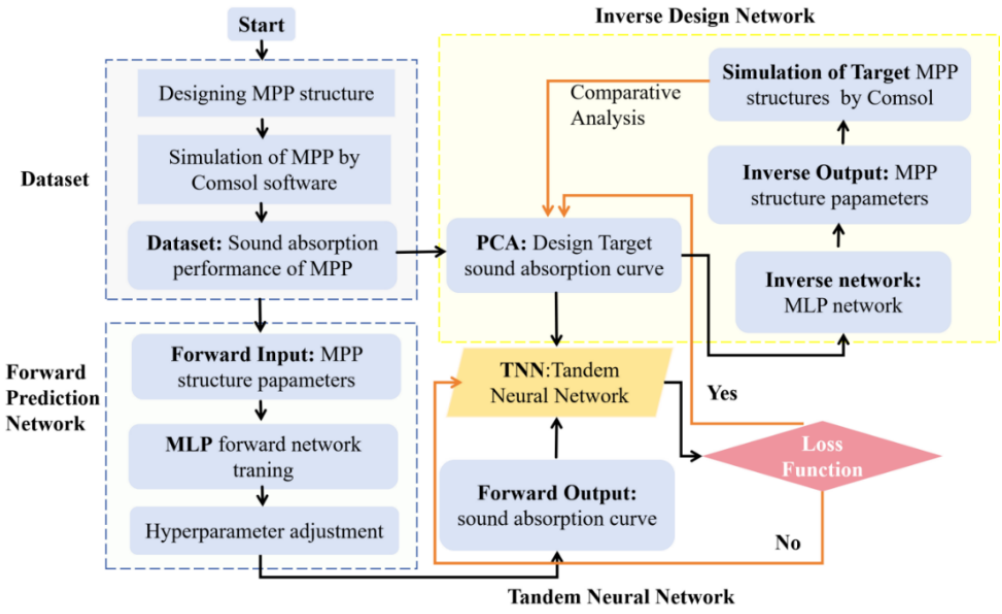

Figure 2. Design Flowchart.

3.1. Dataset construction and partitioning

This dataset includes 2,000 sets of the microstructure and sound absorption coefficient of MPPs, which were obtained by Comsol software and found in previously published articles [25]. The three key structural parameters are the pore size of the micropores, the thickness of the thin panel, and the depth of the back cavity. The changes in these parameters will directly affect the acoustic characteristics of MPPs.

Generally, the diameter of the micro-holes and the thickness of the panel are often less than 1 mm. The aperture ranges from 0.1 mm to 1 mm, the panel thickness from 0.1 mm to 1 mm, and the cavity depth from 1 mm to 10 mm. Each set of data samples includes both the input data and the corresponding label data. In forward prediction, the structure parameters and the sound absorption coefficient are used as input data and output data, respectively. On the contrary, the sound absorption coefficient is the input data in inverse design, and the structure parameters are used as output data.

To ensure the smooth progress of neural network training, during the construction of the dataset, each sound absorption coefficient curve needs to be discretized. To ensure the continuity of the curve, a discrete step size of 10 Hz is taken from 50 Hz to 1,600 Hz. The noise frequency range of much equipment in power plants is within this range, which belongs to the low-frequency range and is also within the experimental testing range of impedance tubes. Thus, the dataset consists of 156 discretized points on the sound absorption coefficient curve, representing the sound absorption coefficient values at frequencies of 50 Hz, 60 Hz, 70 Hz,…, 1,600 Hz, as shown in **Figure 3**. These points accurately depict the relationship between the sound absorption coefficient and the frequency, presenting the sound absorption performance of the MPPs at different frequencies.

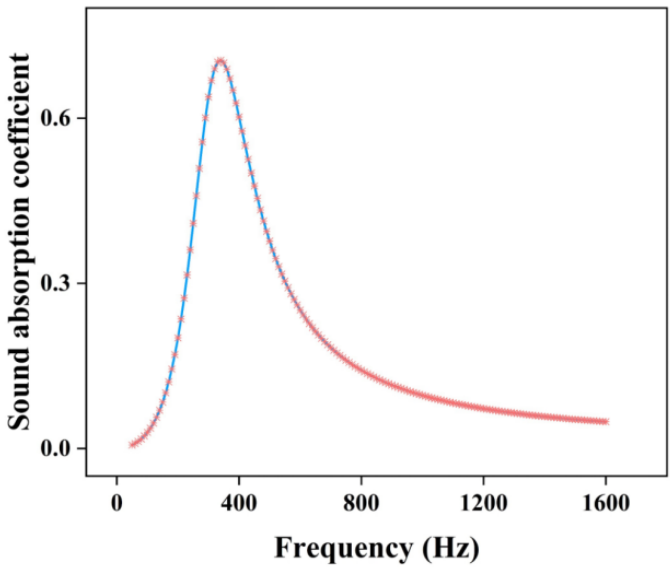

Figure 3. Discrete Acoustic Absorption Coefficient Dataset.

3.2. Forward prediction network

In the forward prediction network, the input data consists of the MPPs' structural parameters. For a single-layer MPP, the thickness of the thin panel (t), perforation diameter (d), and depth of the backing cavity (D) are the three key design parameters. Thus, the input layer of the neural network is set with three neurons, which correspond precisely to these three parameters in order from top to bottom, ensuring that the input information is accurately transmitted into the network for processing. At the output layer, the 156 discrete data points are labeled as label data. This setup allows the forward prediction network to transform the input MPPs' structural parameters into the corresponding discrete absorption coefficient curve.

The dataset is randomly split into training (70%), validation (15%), and test (15%) sets, respectively. The random shuffling of the data sequence breaks the original order, preventing the model from being biased due to the order of the data during training.

Hyperparameter tuning refers to the process of selecting the optimal hyperparameters for an MLP model, typically including the number of hidden layers, layer sizes, batch size, and learning rate. **Table 1** lists the corresponding hyperparameter details for five different MLP models. The performances after hyperparameter adjustment are evaluated with MAE (Mean Absolute Error). Among these five models, the second model demonstrates the best performance on the validation dataset, with an MAE value of 0.0159. The fifth model performs the worst, with an MAE value of 0.0274. Thus, the final MLP model consists of three hidden layers, with 1,024, 512, and 256 neurons, respectively. The learning rate and batch size are set to 0.0001 and 2,000, respectively. This study conducts a grid search on hidden layer configurations, learning rates, and batch sizes. **Table 1** lists five representative configurations evaluated on the validation set.

Table 1. Hyperparameters of the MLP architecture.

Configuration	**1**	**2**	**3**	**4**	**5**
Hidden layer 1	512	1,024	1,024	1,024	1,024
Hidden layer 2	256	512	512	512	512
Hidden layer 3	128	256	512	512	256
Hidden layer 4	-	-	256	256	128
Hidden layer 5	-	-	-	128	-
Learning rate	0.0001	0.0001	0.0001	0.0001	0.001
Batch size	2000	2000	1000	1000	1000
MAE	0.0189	0.0159	0.0169	0.0187	0.0274

Each network layer applies Batch Normalization and the ReLU activation function. Batch Normalization normalizes the input to each layer, accelerating the model's convergence speed and mitigating issues such as vanishing and exploding gradients. The ReLU activation function imparts non-linear expressive power to the network. As the network depth increases, the model's ability to fit complex functions also improves.

During training, the Adam optimizer adaptively adjusts the learning rate based on parameter characteristics, combining the advantages of Adagrad and RMSProp. The loss and accuracy on the training and validation sets are monitored every 10 epochs, and the learning rate is dynamically adjusted if needed. Every 100 epochs, the current model parameters are automatically saved, allowing for fast loading during subsequent training sessions or direct use in inference tasks, ensuring continuity in model training and the effectiveness of the results. The forward prediction network converged after 2,000 iterations. The network converges relatively quickly, indicating that the training process could be further optimized.

To fully verify the predictive performance and superiority of the constructed forward prediction model MLP, this study designed a multi-model comparative experiment, selecting three classic and widely used prediction models: Genetic Algorithm Optimized Support Vector Regression (GA-SVR), Grid Search Optimized

Support Vector Regression (GridSearch-SVR), and Random Forest (RF) as comparison benchmarks. GA-SVR and GridSearch-SVR have improved the generalization ability of traditional SVR models through different optimization strategies, while RF has good anti-interference and robustness with the advantage of ensemble learning. They have strong representativeness in regression prediction tasks and are often used as benchmark models for performance evaluation. **Figure 4** presents scatter plots of predicted versus true values for the four models. Clear differences in prediction performance are observable. The scatter distribution corresponding to the MLP model is closest to the ideal fitting line (y = x), with the lowest degree of dispersion, indicating that its predicted output is highly consistent with the true values. The scatter distribution of GA-SVR, GridSearch-SVR, and RF models is relatively scattered. Among them, the scatter dispersion of the GridSearch-SVR model is particularly prominent. Thus, the visualization result clearly confirms that the MLP model can more accurately capture the intrinsic mapping relationships in the dataset, and its predictive performance is significantly better than the other three compared models.

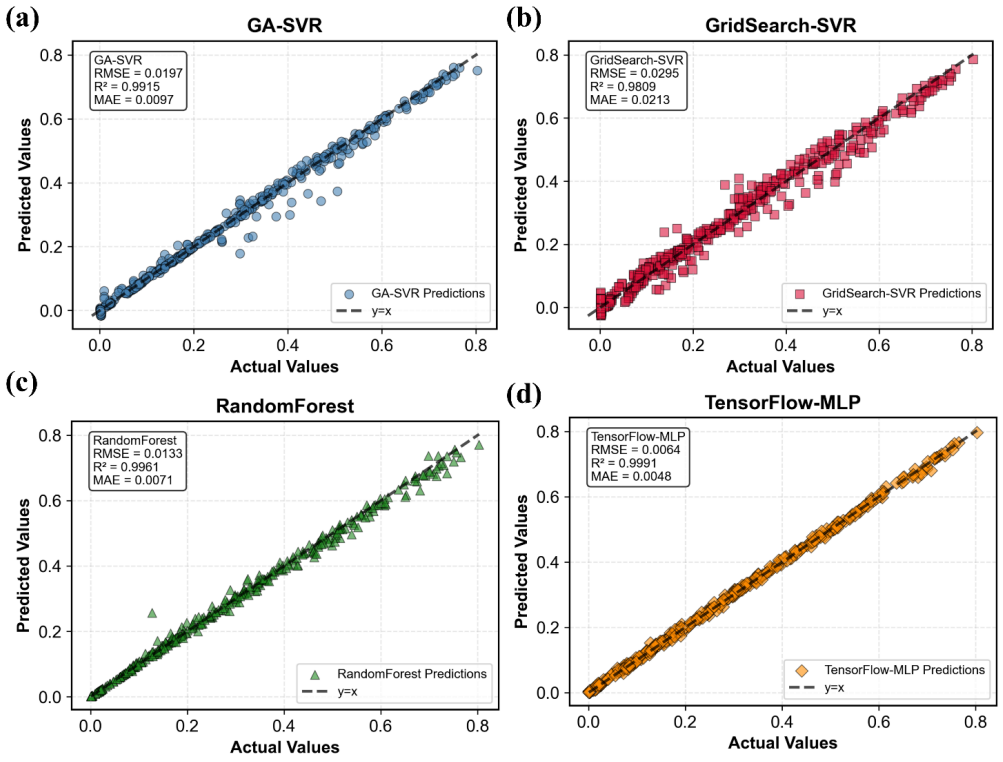

Figure 4. Scatter plot of **(a)** GA-SVR; **(b)** GridSearch-SVR; **(c)** RF; **(d)** MLP.

Quantitatively, the MLP predictions exhibit a correlation coefficient of 0.999 with the true values, compared to 0.9915, 0.9809, and 0.9961 for GA-SVR, GridSearch-SVR, and RF, respectively. The standard deviation of prediction errors for MLP is 0.007, significantly lower than those of the other models (0.020, 0.029, and 0.013). These statistics confirm the visual observation that MLP achieves the most accurate and consistent predictions.

Figure 5 shows the prediction error density distribution of four prediction models. The distribution pattern of errors and core statistical indicators (mean, standard deviation, and skew) can intuitively reflect the differences in prediction accuracy

among various models. The GA-SVR model exhibits a wide error distribution ranging from −0.05 to 0.15, with a mean of 0.003 and a standard deviation of 0.020, indicating a slight positive bias and considerable dispersion. The standard deviation is 0.020 with large fluctuations in error. The skewness is 3.066 with significant positive bias, indicating that samples with large errors are more dispersed. The error distribution interval width of GridSearch SVR is wider, with an error range of −0.10 to 0.10, and the stability is the worst. The mean is the same as GA-SVR, but the standard deviation is 0.029, which is the largest among the four models. The skewness is 0.195, close to symmetry but with strong fluctuations. The error range of RF is between −0.10 and 0.05, with a mean of 0.001, close to 0. The standard deviation is 0.013, which is better than the two SVRs, but the skewness is −1.788. The sample distribution with significant negative bias and small error is scattered. The error range of MLP is concentrated between −0.03 and 0.02, with the narrowest interval. The mean and standard deviation are 0.001 and 0.007, respectively, which are the smallest among the four models. Skewness is −0.046, indicating a nearly symmetrical distribution. It can be seen that the prediction error of MLP is not only close to 0, but also has extremely small fluctuations and a symmetrical and compact distribution.

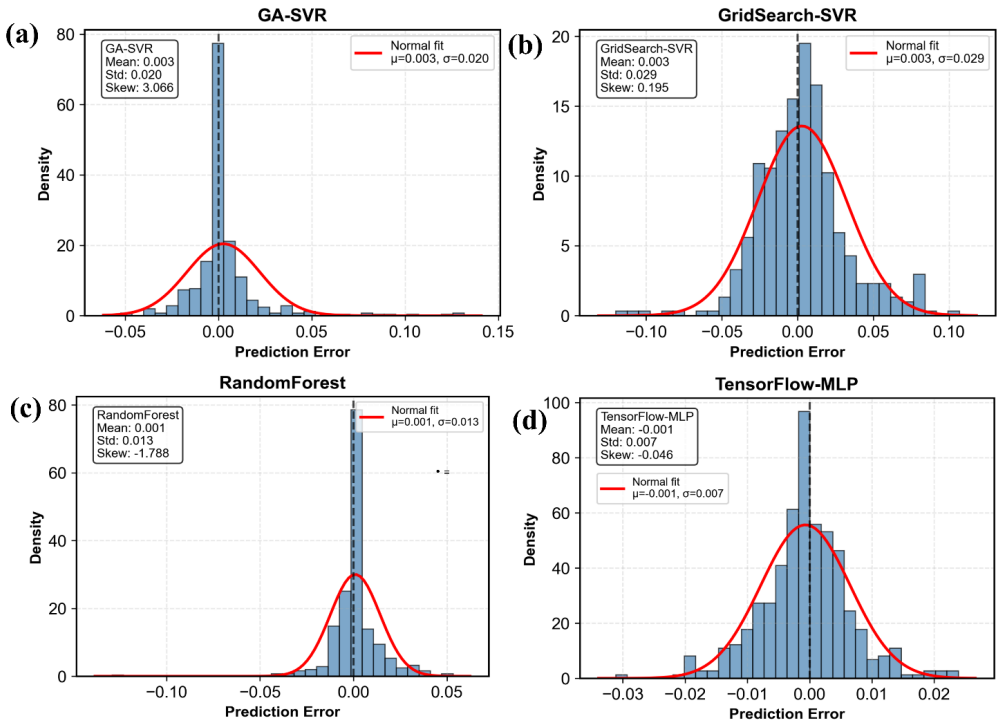

Figure 5. Distribution of prediction error density of **(a)** GA-SVR; **(b)** GridSearch-SVR; **(c)** RF; **(d)** MLP.

Figure 6 presents a bar chart comparing the performance metrics of the four models. The MLP achieves an R^2 of 0.999, RMSE of 0.007, and MAE of 0.005, demonstrating the highest prediction accuracy among all models.

To validate whether the TNN can accurately predict the sound absorption coefficient curve based on input parameters, four random sets of MPP parameter values are selected, as shown in **Table 2**.

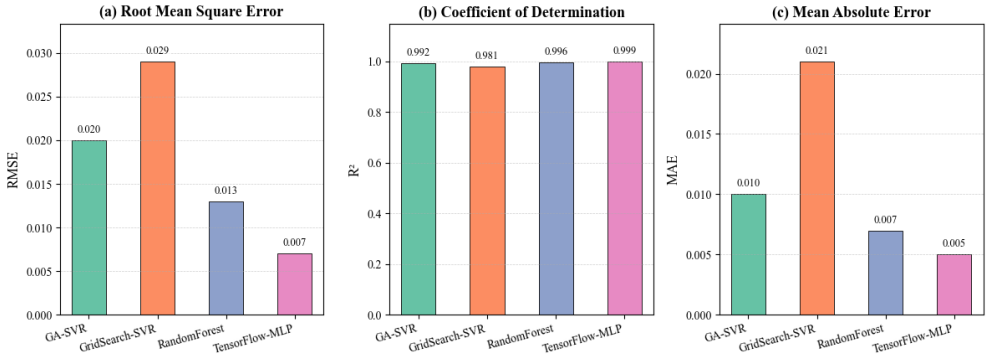

Figure 6. Bar chart comparing: **(a)** R^2; **(b)** RMSE; **(c)** MAE for the four models: GA-SVR, GridSearch-SVR, RF, and MLP.

Table 2. Random MPPs structural parameters.

Structure parameters	Perforating diameter (mm)	Plate thickness (mm)	Cavity depth (mm)
Data 1	1.3	0.5	3
Data 2	0.7	0.7	5
Data 3	1.9	0.9	9
Data 4	0.9	0.6	7

These values are then input into the forward prediction network in a predefined order. Subsequently, the predicted absorption coefficient curves are compared with the original simulation dataset, as shown in **Figure 7**. The blue solid line represents the absorption coefficient calculated using the analytical solution, and the orange dashed line represents the network-predicted absorption coefficient. From the results, it can be seen that there are differences in the peak values of MLP forward prediction results, which may be due to the inability of the forward prediction network to capture the rapidly changing details in continuous equidistant scattered datasets. The rapid rise and fall phase leads to lower peak amplitude prediction. Additionally, the two curves exhibit similar characteristics, including the frequency, width, and magnitude of the absorption peaks. Thus, the overall prediction trend can meet the requirements of inverse design, demonstrating the model's effectiveness and reliability in predicting acoustic properties.

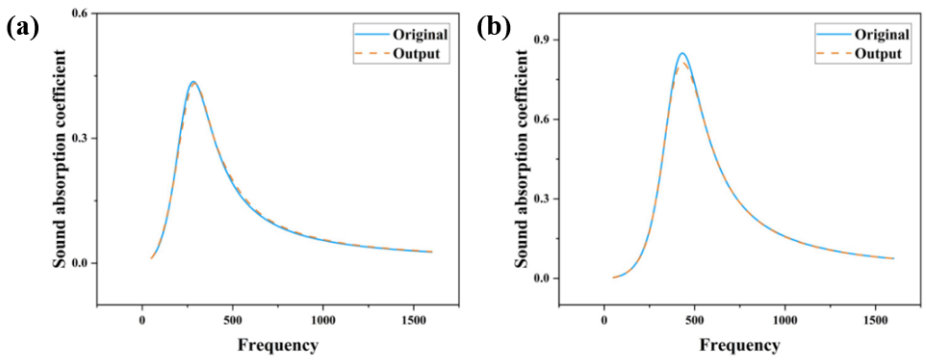

Figure 7. *Cont.*

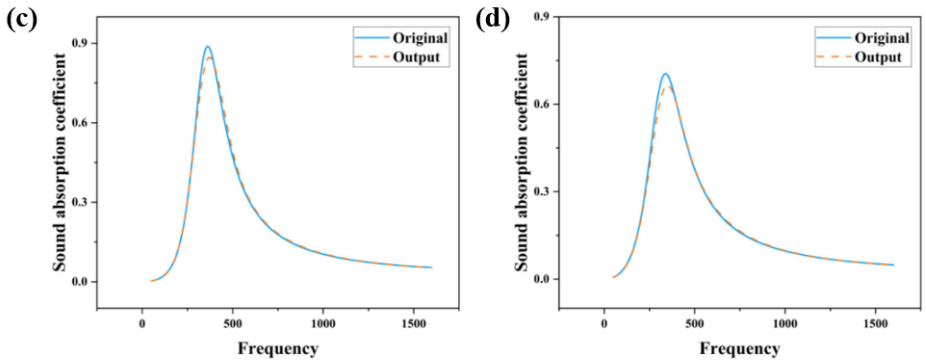

Figure 7. Comparison of MLP Forward Prediction Results and Simulation Results under Different Parameters: **(a)** Data 1; **(b)** Data 2; **(c)** Data 3; **(d)** Data 4.

3.3. Inverse design network

After constructing a forward prediction network that accurately maps structural parameters to acoustic properties, we established an inverse design network to derive structural parameters directly from a target absorption curve. The input is the target absorption coefficient, and we jointly construct the loss function for training TNN with the output attribute of the forward prediction network.

The forward network is pre-trained to learn the hidden relationships between structure and acoustic characteristics, while the inverse network aims to output structures that meet the required acoustic performance. The target property is first input into the TNN inverse design network, and its output design parameters are fed into the trained forward prediction network. A mean squared error (MSE) loss function is then constructed between the target property and the predicted property from the forward network. During TNN training, the parameters of the forward prediction network remain fixed, while only the internal parameters of the inverse design network are updated. Once the loss function converges, the output parameters of the inverse design network are extracted as the designed metamaterial structures.

The observed underestimation of peak values is consistent across all four test cases, with an average relative error of 4.2% at the peak frequency. This systematic bias suggests that the forward MLP, while capturing the overall trend, slightly smooths the sharp resonance features. Future work could address this by incorporating attention mechanisms or using a loss function that places higher weight on peak regions. Nevertheless, the predicted peak frequencies deviate by less than 15 Hz from the true values, confirming that the model accurately captures the resonant behavior.

4. Results and discussion

4.1. Target curve design

To conveniently obtain the required sound absorption coefficient curve, an innovative data generation method is proposed. This method is based on principal component analysis (PCA) and standardization techniques, with the main goal of extracting potentially valuable optimized parameter combinations from current experimental data. The features from the experimental dataset containing 156

absorption coefficient columns are extracted, focusing on the 300 Hz to 600 Hz frequency range as our selection criterion. From the discrete dataset, all absorption coefficient curves are extracted and standardized. The mean of each feature is set to 0 and the standard deviation to 1, respectively, effectively preventing bias caused by varying feature scales and improving model stability and prediction accuracy. By conducting PCA to reduce the dimensionality of standardized data, the top 10 principal components are selected to capture the main trends in the data. The target curve is constructed as a linear combination of the top 10 principal components:

$$a_{target} = \mu + \sum_{i=1}^{10} w_i v_i$$

Where μ is the mean curve of the standardized dataset, v_i are the principal components, and w_i are coefficients manually selected to emphasize high absorption in the 300 Hz–600 Hz range. This approach ensures that the target curve lies within the manifold of physically achievable absorption curves, avoiding unrealistic shapes that might not correspond to any feasible MPP structure.

As shown in **Figure 8**, the first 10 principal components collectively explain **96.3%** of the total variance in the dataset, indicating that they capture the essential modes of variation among the absorption curves. The remaining 3.7% variance is dominated by high-frequency noise and can be safely discarded without sacrificing meaningful information. It can be seen that retaining only the first 10 components to construct the target absorption curve is reasonable, ensuring that the synthesized curve lies within the manifold of physically achievable MPP behaviors.

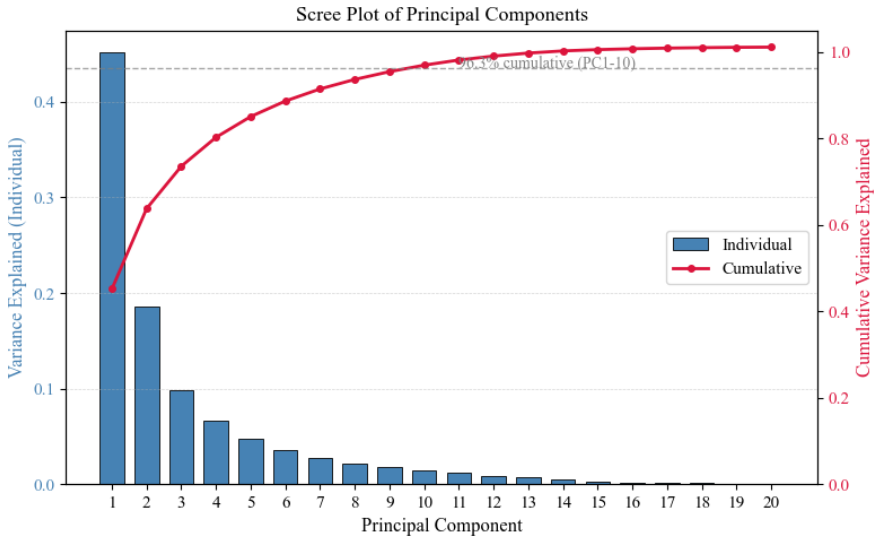

Figure 8. Scree plot with cumulative variance.

In particular, the goal is to achieve an absorption coefficient greater than 0.50 in the 300 Hz–600 Hz range. As shown in **Figure 9**, a specific portion of the curve to achieve the desired absorption effect is highlighted. This feature curve represents key absorption characteristics and trends in this frequency range. To achieve the desired absorption performance, the designed MPPs structure parameters must satisfy specific conditions. In particular, the absorption coefficient curve should form a distinct

absorption peak near 300 Hz–600 Hz, with its peak value approaching 1, indicating near-perfect sound absorption in this frequency band. Beyond 600 Hz–1,600 Hz, the absorption curve follows a gradual decay trend, approaching zero. It reflects the selective absorption characteristics of MPPs across different frequency bands, demonstrating the effectiveness and specificity of the design. After successfully obtaining the target absorption curve, the 156 uniformly distributed data points on the target curve are used as input and fed into the pre-trained TNN model for inverse design.

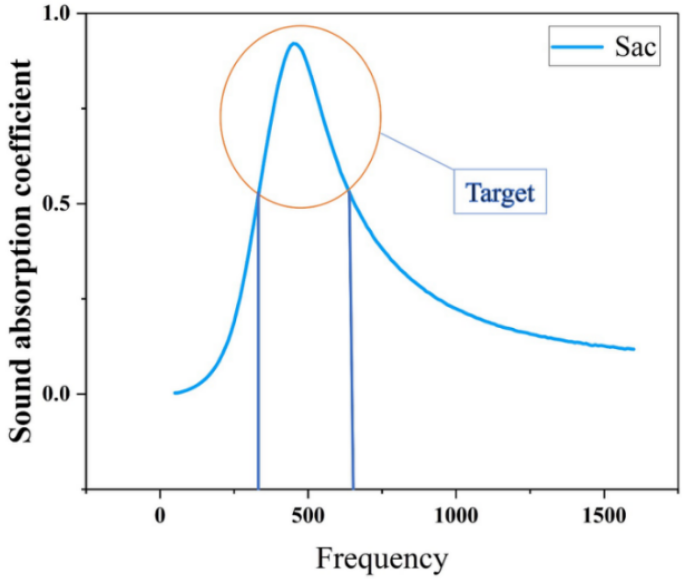

Figure 9. Target Acoustic Absorption Coefficient Curve.

4.2. Inverse design result

In **Figure 10**, the blue design line represents the target sound absorption curve of the inverse design. The structural parameters of perforated panels are designed based on the target sound absorption curve. Then, the structure of the perforated panel is imported into COMSOL software for simulation, and this study obtains the yellow sound absorption curve. It can be seen that the inverse-designed absorption coefficient curve exhibits a high degree of agreement with the target curve. In the critical frequency range of 300 Hz–600 Hz, the two curves demonstrate nearly identical trends, with minimal numerical deviation in the absorption coefficient values. The final MPPs design parameters are: diameter: 0.93 mm, panel thickness: 0.9 mm, cavity depth: 9.9 mm.

In **Table 3**, R^2, MAE, and RMSE of the sound absorption coefficient are 0.997, 0.0097, and 0.0125, respectively. These results confirm that the MPPs' structural parameters determined via inverse design using the TNN successfully meet the stringent requirements for high absorption performance within the specified frequency range. The TNN model has already completed the complex mapping between the absorption coefficient curve and MPPs' structural parameters. By utilizing the powerful nonlinear fitting ability and fast calculation speed of the model, the inverse design process is completed in a short period of time, and the optimal structural parameters are obtained.

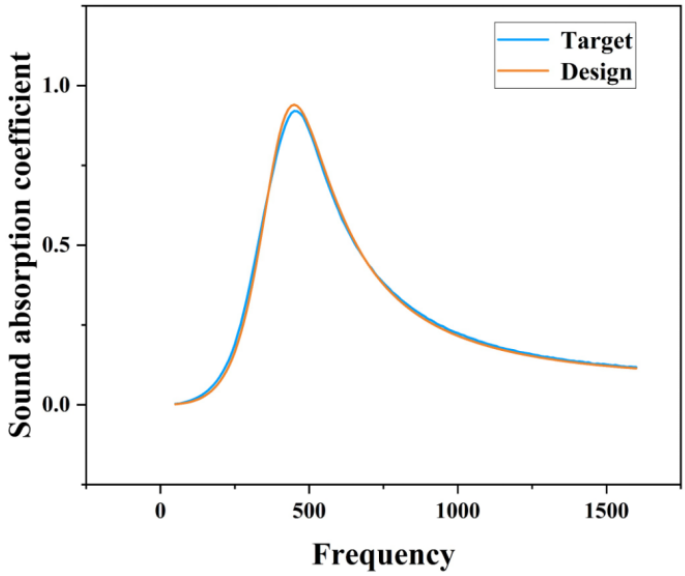

Figure 10. Comparison of Inverse Design Results and Target Acoustic Absorption Coefficient Curve of MPPs.

Table 3. The evaluation index of the inverse design model.

Index	Value
R^2	0.99747
RMSE	0.01254
MAE	0.00971

The close consistency between the inverse-designed and target curves ($R^2 = 0.997$) confirms that the TNN has achieved the inverse mapping. It is worth noting that the designed parameters (d = 0.93 mm, t = 0.9 mm, H = 9.9 mm) are completely within the physically feasible range, demonstrating that the output layer constraints are effective. In practical terms, this means that a noise control engineer could specify a desired absorption peak in the 300 Hz–600 Hz range, which is the critical frequency band for power transformer noise, and obtain manufacturable MPP geometries in milliseconds without any iterative simulation or trial and error. Although demonstrated for single-layer MPPs, the proposed framework can be readily adapted to other acoustic structures, such as multilayer panels or metamaterial-based absorbers, by retraining with appropriate datasets.

5. Conclusion

In this study, due to the complex nonlinear relationship between MPP geometry and acoustic performance, it is difficult to reverse design the target sound-absorbing micro perforated panel (MPP). To address this problem, we propose a cascaded neural network (TNN) framework that can efficiently and accurately reverse engineer single-layer MPPs. This framework consists of two sequentially connected components: a forward multilayer perceptron (MLP) and a reverse design network. To ensure the smooth progress of neural network training, during the construction of the dataset, each sound absorption coefficient curve needs to be discretized. This dataset

takes a point every 10 Hz within the range of 50 Hz to 1,600 Hz. The forward MLP maps three core structural parameters, including perforation diameter, panel thickness, and cavity depth, to the corresponding sound absorption coefficient curve. The comparison results with GA-SVR, SVR, and RF models show that the performance of forward MLP is superior, with an R^2 value of 0.999 and an average absolute error (MAE) of 0.007, highlighting its ability to accurately predict acoustic behavior. By coupling this high-fidelity forward model with a frozen reverse design network, the framework takes the target absorption curve as input and outputs physically feasible structural parameters, where the activation function of the output layer ensures the rationality of the prediction results. The key validation of the TNN framework is achieved through the targeted design of MPPs with distinct absorption peaks in the frequency range of 300–600 Hz. The absorption curve generated by the predicted parameters (diameter 0.93 mm, thickness 0.9 mm, cavity depth 9.9 mm) matched the target with an R^2 of 0.997, thus verifying the accuracy, reliability, and practical applicability of the framework.

Deep learning can achieve efficient and flexible MPP reverse design. Although classical analytical models such as Maa theory provide accurate forward predictions, their inversion of the required absorption curve is not easy, especially for multi-objective or complex structures. The data-driven approach to learning implicit geometric acoustic mapping can be extended to multi-layer or hybrid absorbers. Although the dataset in this article is generated from Comsol calculations rather than experiments, the validity of the data has also been validated before. In addition, feature extraction can be used to reduce high-dimensional inputs (156 frequency points) and improve generalization ability. Overall, this work provides a flexible and data-driven approach for performance-oriented MPP design, with potential applications in areas such as power plant noise mitigation.

Author contributions: Conceptualization, BY and RZ; methodology, XL, TY and TC; validation, XL and TY; formal analysis, TC; investigation, BY and TY; data curation, XL, TY and TC; writing—original draft preparation, XL and TY; writing—review and editing, BY and RZ; supervision, BY and RZ; funding acquisition, RZ. All authors have read and agreed to the published version of the manuscript.

Funding: This work was supported by the National Natural Science Foundation of China (Grant No. 12172210).

Institutional review board statement: Not applicable.

Informed consent statement: Not applicable.

Data availability statement: The data can be obtained by contacting the corresponding author.

Acknowledgment: The authors would like to express their sincere gratitude to the editorial office of Sound & Vibration for granting a partial discount on the Article Processing Charge (APC), which has significantly reduced the financial burden of open-access publication of this study.

Conflict of interest: The authors declare no conflict of interest.

References

1. Liu X, Liu J, He J, et al. Analysis of the characteristics of noise from substations in buildings. Building Services Engineering Research and Technology. 2022; 43(1): 41–56. doi: 10.1177/01436244211035672
2. Chu J, Liang X, Yang Z, et al. A Multi-Layer Micro-Perforated Panel Structure Based on Curled Space for Broadband Sound Absorption at Low Frequencies. Archives of Acoustics. 2023; 529–538. doi: 10.24425/aoa.2023.146813
3. Tang YC, Cheng HD. Analysis and verification of optimization of micro-perforated panels' sound absorption using the Taguchi method. The Journal of the Acoustical Society of America. 2025; 157(4): 3099–3111. doi: 10.1121/10.0036504
4. Wang L, Ma XY, Chen KA, et al. Low frequency sound absorption performance of large sized active micro-perforated panel absorber in free field. Acta Physica Sinica. 2023; 72(6): 064304. doi: 10.7498/aps.72.20222151
5. Li HM, Wu JW, Ya S, et al. Design and study of broadband sound absorbers with partition based on micro-perforated panel and Helmholtz resonator. Applied Acoustics. 2023; 205: 109262.
6. Maa DY. Theory and design of microperforated panel sound-absorbing constructions. Scientia Sinica. 1975; 18(1): 55–71. Available online: https://www.sciengine.com/Math%20A0/doi/10.1360/ya1975-18-1-55
7. Wan XH, Zhang J, Huang Y, et al. Deep learning for Dirac dispersion engineering in sonic crystals. Journal of Applied Physics. 2024; 135(24): 244303. doi: 10.1063/5.0206258
8. Liu Y, He H, Cao Y, et al. Inverse design of TPMS piezoelectric metamaterial based on deep learning. Mechanics of Materials. 2024; 198: 105109. doi: 10.1016/j.mechmat.2024.105109
9. Javadi S, Maghami A, Hosseini SM. A deep learning approach based on a data-driven tool for classification and prediction of thermoelastic wave's band structures for phononic crystals. Mechanics of Advanced Materials and Structures. 2022; 29(27): 6612–6625. doi: 10.1080/15376494.2021.1983088
10. Zhou W, Wang S, Wu Q, et al. An inverse design paradigm of multi-functional elastic metasurface via data-driven machine learning. Materials & Design. 2023; 226: 111560. doi: 10.1016/j.matdes.2022.111560
11. Liu TW, Chan CT, Wu RT. Deep-Learning-Based Acoustic Metamaterial Design for Attenuating Structure-Borne Noise in Auditory Frequency Bands. Materials. 2023; 16(5): 1879. doi: 10.3390/ma16051879
12. He L, Wen Z, Jin Y, et al. Inverse design of topological metaplates for flexural waves with machine learning. Materials & Design. 2021; 199: 109390. doi: 10.1016/j.matdes.2020.109390
13. Zhang H, Liu J, Ma W, et al. Learning to inversely design acoustic metamaterials for enhanced performance. Acta Mechanica Sinica. 2023; 39(7): 722426. doi: 10.1007/s10409-023-22426-x
14. He L, Guo H, Jin Y, et al. Machine-learning-driven on-demand design of phononic beams. Science China Physics, Mechanics & Astronomy. 2022; 65(1): 214612. doi: 10.1007/s11433-021-1787-x
15. Zhang Z, Ye R, Zhu G, et al. Research on sound absorption performance prediction of microporous structures based on integrated learning. Materials Today Communications. 2025; 46: 112866. doi: 10.1016/j.mtcomm.2025.112866
16. Gao N, Wang M, Cheng B, et al. Inverse design and experimental verification of an acoustic sink based on machine learning. Applied Acoustics. 2021; 180: 108153. doi: 10.1016/j.apacoust.2021.108153
17. Mahesh K, Kumar Ranjith S, Mini RS. Inverse design of a Helmholtz resonator based low-frequency acoustic absorber using deep neural network. Journal of Applied Physics. 2021; 129(17): 174901. doi: 10.1063/5.0046582
18. Rodriguez-Guillen D, Díez A, Andrés MV, et al. Inverse design of photonic crystal fibers for dispersion engineering using neural networks. Optics Communications. 2025; 587: 131891. doi: 10.1016/j.optcom.2025.131891
19. Acharige D, Johlin E. Generative tandem neural network for optimization of nanophotonic color splitters. Physica Scripta. 2025; 100(4): 046006. doi: 10.1088/1402-4896/adba19
20. Gupta A, Karahan EA, Bhat C, et al. Tandem Neural Network Based Design of Multiband Antennas. IEEE Transactions on Antennas and Propagation. 2023; 71(8): 6308–6317. doi: 10.1109/TAP.2023.3276524
21. Yan J, Li Y, Yin G, et al. Inverse design on customised absorption of acoustic metamaterials with high degrees of freedom by deep learning. Mechanical Systems and Signal Processing. 2025; 237: 112989. doi: 10.1016/j.ymssp.2025.112989
22. Jiang L, Cao B, Huang A, et al. Accelerated Inverse Design of Multi-Parallel Microperforated Panel Absorbers via Physics-Informed Neural Networks. Applied Sciences. 2025; 15(22): 11955. doi: 10.3390/app152211955

23. Afzal S, Ziapour BM, Shokri A, et al. Building energy consumption prediction using multilayer perceptron neural network-assisted models; comparison of different optimization algorithms. Energy. 2023; 282: 128446. doi: 10.1016/j.energy.2023.128446
24. He J, Chen T, Li G, et al. Embedding physics information into neural networks to enhance the accuracy of star-shaped elastic metamaterial design. Physics Letters A. 2025; 533: 130213. doi: 10.1016/j.physleta.2024.130213
25. Yuan B, You T, Jiang H, et al. Prediction of the sound absorption performance for micro-perforated panel based on machine learning. Journal of Engineering and Applied Science. 2025; 72(1): 27. doi: 10.1186/s44147-025-00598-9